ChemComm

FEATURE ARTICLE

View Article Online
View Journal | View Issue

Cite this: *Chem. Commun.*, 2014, **50**, 9034

Studying the dynamic behaviour of porphyrins as prototype functional molecules by scanning tunnelling microscopy close to room temperature

H. Marbach* and H.-P. Steinrück

Received 7th March 2014,
Accepted 11th May 2014

DOI: 10.1039/c4cc01744g

www.rsc.org/chemcomm

Scanning tunnelling microscopy (STM) enables us to directly observe the dynamic behaviour of organic molecules on surfaces. While imaging atoms and molecules using STM is certainly fascinating by itself, corresponding temperature-dependent measurements allow for the quantitative determination of the energetics and kinetics of the underlying molecular surface processes. Herein, we review recent advances in the STM investigation of the dynamic behaviour of adsorbed porphyrins at and close to room temperature. Three different case studies are discussed, providing insight into the dynamics of diffusion, rotation, reaction, and molecular switching at surfaces, based on isothermal STM measurements. The reviewed examples demonstrate that variable temperature STM can be a suitable tool to directly monitor the dynamic behaviour of individual adsorbed molecules, at and close to room temperature. Free base porphyrins on Cu(111) proved to be particularly suitable for these studies due to the strong bonding interaction between the iminic nitrogen atoms in the porphyrin macrocycle and the Cu substrate atoms. As a consequence, the corresponding activation energies for surface diffusion, self-metalation reaction and conformational switching are of a magnitude that allows for monitoring the processes at and around room temperature, in contrast to most previous studies, which were performed at cryogenic temperatures. The kinetic analysis of the surface diffusion and self-metalation was performed using an Arrhenius approach, yielding the corresponding activation energies and preexponential factors. In contrast, the conformational switching process was analysed in the framework of transition state theory, based on the Eyring equation. This approach provides a more detailed insight into interpretable thermodynamic potentials, *i.e.*, the enthalpic and entropic contributions to the activation barrier. The analysis shows that at room temperature the adsorption and switching behaviour of the investigated free base porphyrin on Cu(111) is dominated by entropic effects. Since the entropic energy contribution vanishes at low temperatures, the importance of experiments conducted at temperatures close to room temperature is emphasized.

1 Introduction

With the invention of the scanning tunnelling microscope (STM) in the early 80's of the last century[1] the direct real space observation of atoms and molecules on extended surfaces of solids became possible. Based on its unparalleled capabilities, the STM was quickly established as a powerful tool in fundamental sciences and is nowadays a standard instrument in laboratories all over the world. Among manifold STM-based research activities, the investigation of large organic molecules on surfaces has become a vivid field in science with the vista to engineer functional devices.[2,3] Specific interactions between absorbed molecules and/or with the underlying substrate often trigger peculiar adsorption behaviours like the self-assembly into long range ordered arrays or the occurrence of individual isolated molecules. Due to their versatility, the molecules from the "porphyrin family" are considered as ideal building blocks for the generation of functional molecular devices: they combine a rigid planar framework as a structure-forming element with an intrinsic functionality, which is mainly determined by the coordinated metal center.[4] The importance of porphyrins is highlighted by their omnipresence as main functional building blocks in nature[5]—examples are iron porphyrin in heme[6] or magnesium porphyrin in chlorophyll[7]—but also due to their application in sensor[8,9] and solar cell technology.[10–15] The enormous potential of porphyrins for the fabrication of tailor-made functional molecular architectures on well-defined substrates has stimulated significant activities in fundamental research.[4,16–32]

In this contribution, we review recent advances in the understanding of the dynamic behaviour of porphyrins, as representatives

Lehrstuhl für Physikalische Chemie II, Egerlandstrasse 3 and Interdisciplinary Center for Molecular Materials (ICMM), Friedrich-Alexander-Universität Erlangen-Nürnberg, D-91058 Erlangen, Germany. E-mail: hubertus.marbach@fau.de

of organic molecules, adsorbed on a Cu(111) single crystal surface in ultra-high vacuum (UHV). Based on temperature-dependent measurements of individual molecules, the kinetics and energetics of diffusion[33,34] and rotation,[34] of the so-called self-metalation reaction[35,36] and finally of conformational switching of particular free base porphyrins[37] can be determined. Even though these processes appear to be very different at first glance, they can all be regarded as activated processes, as schematically sketched in Fig. 1. The standard method to extract quantitative information from temperature-dependent data of such surface processes is the Arrhenius analysis. Svante Arrhenius developed his famous equation on a purely empirical basis and published it at the end of the 19th century.[38]

The general form of the Arrhenius equation is:

$$r(T) = A \cdot \mathrm{e}^{-\frac{E}{k_\mathrm{B}T}}$$

with $r(T)$ being the temperature-dependent rate, A the so-called preexponential factor and E the activation barrier or energy (see Fig. 1) of the investigated process (k_B: Boltzmann constant, T: temperature). While the activation energy E is intuitively accessible and the exponential dependency can be comprehended by regarding the Maxwell–Boltzmann statistics, the interpretation of the preexponential factor A is somewhat more difficult. For first order processes, to which all processes discussed in this feature article belong to, the dimension of A is s^{-1}. Therefore, A is also often referred to as the frequency factor, somewhat naively implying that the involved molecule vibrates with a frequency given by A in the relevant potential; in some cases, this interpretation can be correct, but in others it is certainly misleading.

An alternative and fully comprehensible interpretation of the preexponential factor was deduced in the frame of the transition state theory (TST) by Eyring and co-workers.[39] In TST, the activation barrier (see Fig. 1) is defined as the difference in Gibbs energy, $\Delta G^{\#}$, of the initial and the transition states.

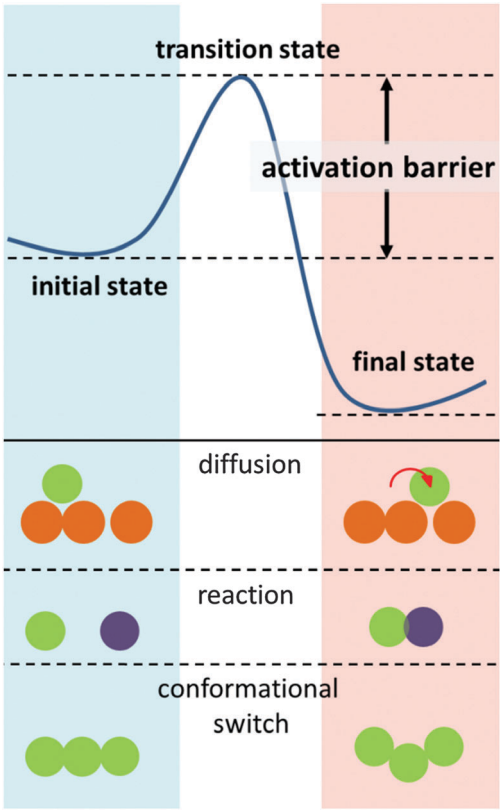

Fig. 1 Generalized energy scheme for an activated process (top), and three corresponding examples (diffusion, reaction and conformational switching).

With the introduction of the thermodynamic potential $\Delta G^{\#}$ and by considering the Gibbs–Helmholtz equation, $\Delta G^{\#} = \Delta H^{\#} - T\Delta S^{\#}$, the temperature-dependent rate follows as

$$r(T) = \left(\frac{k_\mathrm{B}T}{h}\right) \cdot \mathrm{e}^{-\frac{\Delta G^{\#}}{k_\mathrm{B}T}} = \left(\frac{k_\mathrm{B}T}{h}\right) \cdot \mathrm{e}^{\frac{\Delta S^{\#}}{k_\mathrm{B}}} \mathrm{e}^{-\frac{\Delta H^{\#}}{k_\mathrm{B}T}}$$

H. Marbach

Dr Hubertus Marbach studied physics at the TU Dortmund and Ruhr University Bochum (Diploma, 1997); thereafter, he joined Prof. Dr Ronald Imbihl at the Leibnitz University Hannover for his PhD (2002, with highest praise); from 2002 to 2004 he was a postdoc at the University of Pittsburgh with Prof. Dr John T. Yates Jr. In 2004, he joined the Chair of Physical Chemistry II at the University of Erlangen-Nürnberg as a group leader and established the working group "Microscopy and Nanolithography"; in 2010 he received his Habilitation. Current research topics: surface science with porphyrins and the fabrication of functional nanostructures with a focused electron beam.

H.-P. Steinrück

Prof. Dr Hans-Peter Steinrück (born in 1959 in Austria) studied physics at the TU Graz (Diploma in 1983; PhD in 1985), was a postdoc at Stanford University (1985/1986), and received his Habilitation at the TU Munich in 1992. After a sabbatical at Rutgers University, he became Professor of Experimental Physics at the University of Würzburg in 1993; since 1998, he has held a chair of Physical Chemistry at the University of Erlangen-Nuremberg. Current research topics cover: surface science with porphyrinoids, in situ studies of surface reactions, ionic liquid surface science, hydrogen carrier molecules, and chemically modified graphene layers. www.chemie.uni-erlangen.de/steinrueck

the so-called Eyring equation. A more detailed discussion of this equation will be given in Section 4 below. Nevertheless, one can already state here that the analysis of the temperature-dependence of the reaction rate gives direct access to the contributions of the thermodynamic potentials $\Delta H^{\#}$ and $T\Delta S^{\#}$ to the Gibbs energy, $\Delta G^{\#}$. Since the entropic contribution, $T\Delta S^{\#}$, scales with T, it is immediately clear that it vanishes at low temperatures. Consequently, in low temperature (LT) STM measurements entropic effects practically do not play a role. Therefore, such effects can only be studied by performing experiments at higher temperatures. In turn, if one performs experiments at higher temperatures, entropic contributions should be considered in order to obtain a detailed understanding of the energetics of a process. Herein, we review results obtained at and close to room temperature (RT), not only because such measurements are closer to realistic conditions for applications, but also since they allow for investigating the role of entropic effects. The comparison of the Arrhenius equation and the Eyring equation reveals that the preexponential factor A linearly depends on T and contains a term that depends on the entropy difference between initial and transition state, $\Delta S^{\#}$:

$$A = \left(\frac{k_B T}{h}\right) \cdot e^{\frac{\Delta S^{\#}}{k_B}}$$

Note that for $\Delta S^{\#} = 0$ and a temperature of 480 K, A equals 10^{13} s^{-1}, which is the value typically used as the first order approximation of the preexponential factor, if no other information is available.

In the first two examples discussed below, *i.e.*, for diffusion and rotation, and for the self-metalation reaction on surfaces, the kinetic analysis is performed using the Arrhenius equation, as typically done in surface science. For the third example, which addresses conformational switching of molecules on surfaces, the analysis is based on the Eyring equation, because a detailed insight into the thermodynamic potential was required in order to understand the observed complex behaviour.

2 Diffusion and rotation of 2HTPP

The diffusion dynamics of adsorbates on surfaces are of fundamental interest in surface science and constitute the basis for the self-assembly of functional molecular architectures in a bottom-up approach.[16,40] STM has proven to be a suitable tool for the investigation of surface migration and the determination of the corresponding kinetic parameters. While initially mainly the surface diffusion of atoms or small molecules on metal surfaces[41–45] was addressed, in the last decade large organic molecules were also investigated;[46] these studies include decacyclen and hexa-*tert*-butyldecacyclene on Cu(111),[47] dithioanthracene on Cu(111),[48] 4-*trans*-2-(pyrid-4-yl-vinyl) benzoic acid on Pd(110),[49] C_{60} on Pd(110),[50] tris-(2-phenylpyridine)iridium(III) on Cu(111),[51] and 2*H*-tetrapyridylporphyrin (2HTPyP) on Cu(111).[33] The latter study by Eichberger *et al.* represents the first example of the direct observation of the unidirectional motion of porphyrins at 300 K and above, *i.e.*, at comparably high temperatures, by STM. The fact that this was possible is especially remarkable, since porphyrins usually rapidly diffuse on the time scale of STM at RT and thus cannot be imaged as individual molecules.[52] However, for 2HTPyP and also for the very similar 2*H*-tetraphenylporphyrin (2HTPP) (which will be discussed in detail below) the molecules can indeed be imaged as isolated individual entities at RT on Cu(111).[33,34,36,37,53–58] The reason for the very peculiar adsorption behaviour of these free base porphyrins on Cu(111) is a strong site-specific attractive interaction between the iminic nitrogen atoms of the porphyrin macrocycle and the Cu substrate atoms; this specific interaction was already suspected in ref. 33 and 55 and later on verified by XPS.[58] In the following, the specific role and interplay of adsorbate–substrate and adsorbate–adsorbate interactions of different tetraphenylporphyrins (2HTPP and CoTPP) on Ag(111) and Cu(111) will be discussed. The STM images in Fig. 2a and b illustrate the island formation, *i.e.*, the self-assembly behaviour of tetraphenylporphyrins (TPP) on Ag(111) at RT. For TPPs without a central metal atom, *i.e.*, 2HTPP, and also for metallotetraphenylporphyrins with various central metal atoms (*e.g.*, Co, Fe, Zn, Ni), the formation of square arrays with a lattice constant of 1.40 ± 0.05 nm is always observed.[52] In addition, different TPP species (*e.g.*, 2HTPP and CoTPP) statistically intermix in the square arrangement without any detectable spatial correlation. The driving force for the formation of this supramolecular order is a mutual stabilization mediated by so-called T-type interaction between the phenyl groups of neighbouring molecules.[52,59] The same behaviour, namely the island formation with a square lattice from a certain coverage on, is also observed for CoTPP and CuTPP on Cu(111).

A completely different behaviour is observed for 2HTPP on Cu(111), as is evident from the STM image depicted in Fig. 2c, where no island formation is found at low and medium coverages. In contrast, individual molecules can be identified; this behaviour is attributed to the above-mentioned site-specific coordinative bond between the iminic nitrogen atoms of the porphyrin macrocycle and the Cu atoms. As a consequence of this interaction, the molecule is literally pulled towards the surface, as indicated in Fig. 2e, which results in a nearly flat conformation with the phenyl rings almost parallel to the surface; this geometry leads to the characteristic appearance of the molecule with two long parallel protrusions, which is shown in Fig. 2e. The orientation of the phenyl rings nearly parallel to the surface effectively inhibits the mentioned attractive T-type interactions between neighbouring molecules, which explains why 2HTPP does not form two-dimensional islands on Cu(111). We also want to mention a somewhat different interpretation, given by Rojas *et al.*, who proposed a considerable charge transfer from the Cu(111) substrate to the 2HTPP which results in repulsive dipole–dipole interaction between the free base porphyrins.[54,60] However, Buchner *et al.* found no indications of such a massive charge transfer; such indications would be the asymmetric appearance of 2HTPP upon switching the polarity of the bias voltage or reduced residence times and changed velocities for 2HTPPs at small intermolecular distances.[55] Still, one cannot rule out that both proposed effects might contribute to the observed behaviour.

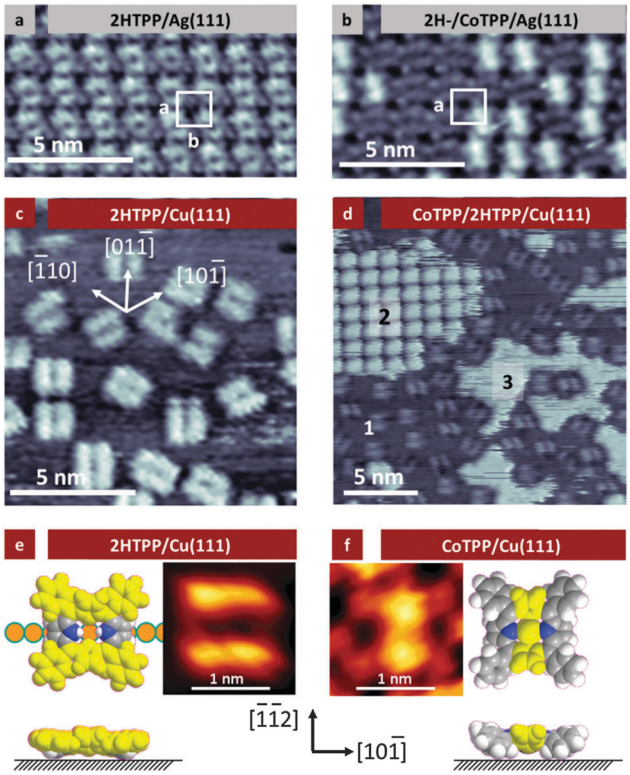

Fig. 2 Constant current RT STM images: (a) a monolayer of 2HTPP on Ag(111) (U = + 0.45 V, I = 25 pA); (b) intermixed 2HTPP–CoTPP monolayer with a ratio of 2 : 1 on Ag(111); the bright long protrusions correspond to CoTPPs; (U = −1.35 V, I = 35 pA); (c) 2HTPP on Cu(111) (U = −0.77 V, I = 26 pA); (d) mixed 2HTPP–CoTPP coverage on Cu(111) (U = −1.94 V, I = 27 pA). Molecules indicated with 1 are individual 2HTPPs, the square array marked with 2 is a self-assembled square array from CoTPP. The bright regions labelled with 3 are highly mobile CoTPP molecules. (e) STM image of an individual 2HTPP with the corresponding scaled space-filling model (U = −1.49 V, I = 30 pA). A closed packed Cu atomic row is indicated, highlighting the coordinative bond between the iminic nitrogen atoms of 2HTPP and the copper substrate atoms. (f) STM image of a single CoTPP with the corresponding scaled space-filling model (U = −1.48 V, I = 27 pA). All bias voltages given in the work at hand refer to the sample. The parts marked yellow in the models are the topographically highest parts of the molecules. (Adapted with permission from Buchner *et al.*[55] Copyright 2011 Wiley.)

To illustrate the different adsorption behaviour of 2HTPP and metalloporphyrins at submonolayer coverages on Cu(111), a mixture of 2HTPP and CoTPP was deposited on Cu(111). The corresponding STM image in Fig. 2d shows a phase separation of the two species. 2HTPPs appear as isolated molecules, as in pure 2HTPP layers. On the other hand, CoTPPs form well-ordered islands with a square unit cell. The appearance of CoTPP in the STM image with submolecular resolution in Fig. 2f is dominated by the two pyrrole groups, which are bent away from the surface. This specific appearance of individual TPPs in STM is due to a saddle-shape distortion of the molecule and is well established in the literature.[52,59]

In Fig. 2d, the regions with isolated 2HTPP molecules are labelled with "1" and regions, where CoTPP forms islands with "2". In corresponding RT STM movies one occasionally observes CoTPP molecules which attach at and detach from the rim of the island, indicating a high mobility of isolated CoTPPs. Indeed, the bright, unstructured regions labelled with "3" in Fig. 2d are assigned to CoTPP molecules diffusing fast under the STM tip. This illustrates that CoTPPs are also present in a 2D gas phase on the surface. Such molecules are not directly visible as individual molecules in the STM under the actual imaging conditions due to their high mobility.[61–63] The observed effective phase separation of 2HTPP and CoTPP on Cu(111) results from the fact that the adsorption of the free base 2HTPP is dominated by molecule–substrate interactions, while the supramolecular arrangement of CoTPP is caused by attractive molecule–molecule interactions.

Fig. 3 provides a more detailed insight into the specific adsorption behaviour of 2HTPP on Cu(111). The figure shows that only three different azimuthal orientations are found, which are rotated with respect to each other by 120°. This means that the molecules are aligned along one of the three symmetry-equivalent densely packed substrate ⟨110⟩ directions, which are indicated as white arrows in the right lower corner of Fig. 3a. The observation of isolated 2HTPPs at RT indicates a low mobility compared to, *e.g.*, CoTPP on Cu(111), which cannot be imaged as individual molecules at this temperature (see above).

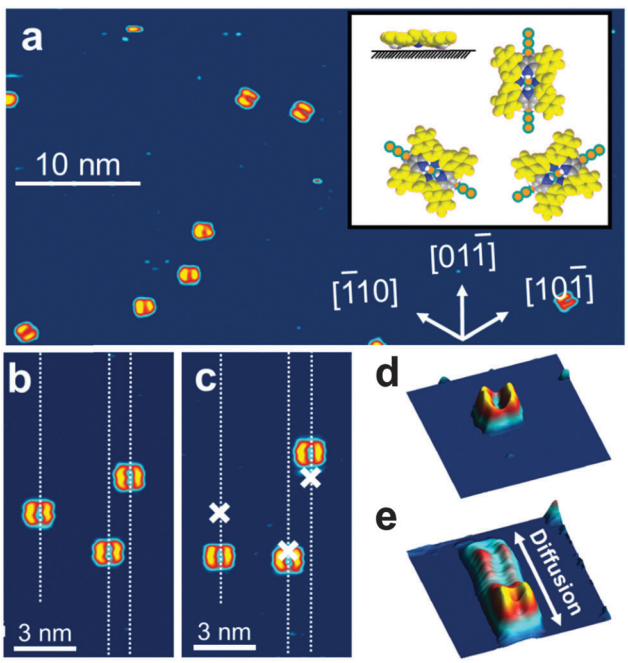

Fig. 3 (a) Constant current STM image of 2HTPP on Cu(111) at low coverage, obtained at 301 K. The space-filling model in the inset exhibits the proposed intramolecular saddle-shape conformation and depicts the orientation relative to the Cu surface atoms along the surface ⟨110⟩ directions. (b) and (c) Subsequently recorded images of the same scan area: the position of the molecules in (b) is highlighted in (c) with crosses; the dashed white lines indicate the directions of the one-dimensional diffusion. (d) Pseudo three-dimensional STM image of a single 2HTPP and (e) the average STM frame of the corresponding STM time lapse movie (37 images with 20 seconds acquisition time each), with the elongated shape emphasizing the unidirectional diffusion. [(a–e) U = −1.49 V, I = 30 pA]. (Adapted with permission from Buchner *et al.*[34] Copyright 2011 American Chemical Society.)

Next, the dynamic behaviour of 2HTPP on Cu(111) is reviewed in detail. In the two subsequently recorded STM images of the same surface region in Fig. 3b and c (sample temperature: 301 K; time interval: ~265 s) three molecules with identical orientation can be recognized. When comparing the two images, it becomes evident that the positions of two of the molecules changed in a very specific way (note that the positions of the molecules in Fig. 3b are indicated by white crosses in Fig. 3c):

For both, one-dimensional displacements along the high-symmetry substrate direction occurred, along which the molecules were aligned (indicated with dash-dotted lines). The one-dimensional motion can be even better illustrated by inspecting the average frame of a corresponding STM movie (37 images) acquired at 301 K in Fig. 3e. The average frame appears to be an elongated version of the two parallel protrusions of the single frame in Fig. 3d. This behaviour indicates a unidirectional motion of 2HTPP on Cu(111). Considering the moderate displacement per time (*e.g.*, far below 5 nm per 265 s in Fig. 3c), the tracing of individual 2HTPP becomes possible by STM, even at the comparably high temperature of 301 K. This enables temperature-dependent measurements of the displacement of individual porphyrins at around RT. When performing such measurements, one needs to ensure an undistorted thermally induced motion of the molecules, *i.e.*, the influence of the STM measurements must be ruled out or at least minimized. In this context, it is beneficial that the 2HTPP–Cu(111) system can be imaged with a high tunnelling resistance ($U \sim 1.5$ V, $I \sim 30$ pA, $R \sim 50$ GΩ), which allows us to avoid tip induced effects. Note that diffusion measurements by STM found in literature are typically carried out at tunnelling resistances in the range of 1–10 GΩ.[33,47–49,64] Since the tunnel resistance in the experiments by Buchner *et al.*[34] is even higher, *i.e.*, the tip-substrate interaction is lower, a significant influence of the STM measurement on the thermally induced diffusion can be practically ruled out. In addition, no influence upon changing image size, scanning speed and the fast scan direction (vertical/horizontal) was reported. To avoid the influence of intermolecular interactions (collisions), the 2HTPP coverage was kept sufficiently low in the corresponding experiments.

Following this approach, STM movies at different temperatures between 280 and 345 K were acquired (see ESI of ref. 34). These movies comprise roughly 50 images with an acquisition time of 20–40 s per image, allowing for the analysis of roughly 2500 diffusion events. Fig. 4a–d present the average frames (superposition of the image series) at four temperatures. To illustrate the movement of the 2HTPPs the position of each molecule was marked in the images with a specific colour. The resulting traces of the individual molecules illustrate the temperature-dependent diffusion behaviour. Briefly, the behaviour at the different temperatures in Fig. 4 can be described as follows: 280 K (a): 2HTPP molecules are confined to their adsorption sites, *i.e.*, the circular or only slightly elongated dots indicate that no detectable movement occurs in the timeframe of the experiment; 301 K (b): unidirectional trajectories along one of the three high-symmetry directions of the surface are observed; 315 K (c): unidirectional trajectories with increased length are seen, with occasional changes of the direction of the trajectories by ±120°, *i.e.*, to one of the other high-symmetry substrate axes; 330 K (d): a further increase of the diffusion length and more frequent directional changes are found. For 345 K (not shown), the molecular diffusion is so fast that changes in the images already occurred on a time scale shorter than required to obtain one image, and the displacements were partly larger than the scan area. These data can therefore not be considered in the kinetic analysis. The quantitative analysis was performed using the procedure described by Eichberger *et al.*:[33] in a first step, the molecular displacements between consecutive images were evaluated for each temperature. From these data, the mean square displacement $\langle(\Delta x)^2\rangle$ and correspondingly the hopping rate[65] $h(T) = \langle(\Delta x)^2\rangle/(\langle\lambda\rangle^2 t)$ for each of the investigated temperatures were determined (λ is the jump length, *i.e.*, the lattice constant of 2.55 Å along the ⟨110⟩ directions and t is the corresponding time interval).

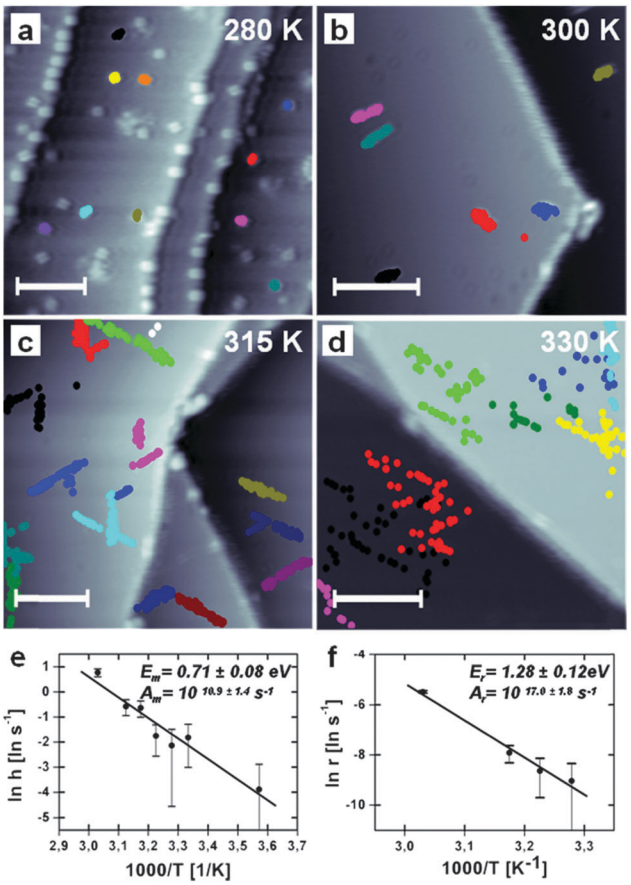

Fig. 4 (a–d) Average frames of STM movies of 2HTPP on Cu(111) between 280 and 330 K (scale bar = 10 nm). The positions of the molecules were color-coded in each single STM image and then superimposed over the corresponding STM average frames [(a) $U = -1.51$ V, $I = 29$ pA; (b–d) $U = -1.49$ V, $I = 30$ pA]. (e) Arrhenius plot of the hopping rates *vs.* temperature. (f) Arrhenius plot of the rotational change of the diffusion direction. (Adapted with permission from Buchner *et al.*[34] Copyright 2011 American Chemical Society.)

The data show a linear dependence, consistent with the Arrhenius equation for

surface diffusion, $h(T) = A_m \exp[-E_m/(k_B T)]$.[47,49,65] The slope of the linear fit in Fig. 4e yields the migration barrier for diffusion of 2HTPP on Cu(111), $E_m = 0.71 \pm 0.08$ eV. From the ordinate intercept the preexponential factor is determined to be $A_m = 10^{10.9\pm1.4}$ s^{-1}. These values are to be compared with the values of $E_m = 0.96 \pm 0.09$ eV and $A_m = 10^{12.0\pm1.4}$ s^{-1} for 2HTPyP on Cu(111) reported by Eichberger *et al.*[33] The larger migration barrier is attributed to an additional interaction of the nitrogen atoms in the pyridyl side groups of 2HTPyP with the Cu substrate. Overall, it can thus be concluded that the contribution from the iminic nitrogen atoms dominates the diffusion behaviour. Eichberger *et al.* also reported another interesting observation, that is, strongly enhanced mobility of 2HTPyP dimers; these dimers are presumably formed by a linkage of two 2HTPyP molecules *via* a Cu atom, connecting the nitrogen atoms in the pyridyl groups. The Arrhenius analysis of the diffusion of the dimers yielded $E_m = 0.94 \pm 0.03$ eV and $A_m = 10^{14.0\pm0.5}$ s^{-1}. Since the activation energies, E_m, of monomer and dimer diffusion are identical in the margin of error, the much higher mobility of the dimer is solely related to the higher preexponential factor and thus (as discussed in the introduction) must be due to entropic effects. This observation was attributed to the fact that upon dimer formation the TPyP internal degrees of freedom (energetically low lying bending and rocking modes) are constrained as compared to the individual molecule.[33] This nice example convincingly demonstrates that entropic effects can play an important role in activated processes.

In a next step, the temperature-dependence of the rotation of the migration direction by $\pm 120^\circ$ is analysed between 305 and 330 K (at lower T, there are too few events for a reliable statistical analysis). The corresponding Arrhenius plot for the rotation rate $r(T) = A_r \exp[-E_r/(k_B T)]$ in Fig. 4f shows again a linear behaviour, and the corresponding fit yields a rotation activation barrier of $E_r = 1.28 \pm 0.12$ eV and a preexponential factor of $A_r = 10^{17.0\pm1.8}$ s^{-1}. The much higher barrier for rotation than for unidirectional motion is attributed to the very pronounced site-specificity of the N–Cu interaction, in combination with a complex change of the molecular conformation during the rotation event. If one interprets the preexponential factor of the rotation literally as a frequency factor and thus as the frequency of the molecular vibration (frustrated rotation), the corresponding value appears to be unreasonable high at first glance. However, when considering that the preexponential factor reflects the entropy gain from the initial to the transition state, one could speculate that additional degrees of freedom (*e.g.*, nearly free azimuthal rotation in the transition state) could account for the observed high value. Indeed, for the desorption of "large" organic molecules (comparable to 2HTPP), similar and even higher frequency factors were reported in literature.[66–69] A more detailed discussion of such effects follows in Section 4.

Prior to the results just mentioned, rotational hopping of porphyrins was found only when the molecules are embedded in a closely packed supramolecular framework, at temperatures well below 100 K. Examples are zinc-octaethylporphyrin on Cu(111) with an rotational activation energy of 0.17 eV[70] and zinc-tetrakis-(di-*tert*-butylphenyl)porphyrin with an activation energy of 0.24 eV.[24] Since for both metal complexes all nitrogen atoms coordinate to the central Zn ion, no pronounced site-specificity, as found for 2HTPP, is expected. Consequently, the rotational dynamics of both metalloporphyrins should be governed by lateral molecule–molecule interactions rather than by molecule–substrate interactions.[33,71] Thus, 2HTPP on Cu(111) represents the first example of the rotation of individual porphyrin molecules on a pristine surface and the evaluation of the corresponding rotation barrier. The results described in this section demonstrate that the investigated system is especially suitable for dynamic STM studies, owing to the fact that the pronounced site-specificity of the adsorbate–substrate interaction of 2HTPP on Cu(111) yields an untypically large surface corrugation. This allowed us to directly trace the dynamics of individual molecules at room temperature. This peculiar behaviour is in contrast to the high mobility of corresponding metalloporphyrins, *e.g.*, CoTPP or CuTPP, and will enable us to investigate the kinetics of a surface-confined metalation reaction in the next chapter.

3 Self-metalation of 2HTPP with Cu substrate atoms

With the first observation of surface-mediated *in situ* metalation of porphyrins a new route for the controlled fabrication of functional molecular architectures has been established,[61,72,73] which stimulated significant further research activities.[4,32,35,36,56,58,72–85] It is nowadays well established that metalloporphyrins can be synthesised readily on a metal surface by the reaction of a corresponding free base porphyrin with an "available" metal atom. The respective metal atom can be provided on the surface by pre- or post-deposition, or originate from the surface itself. Depending on the metal, this *in situ* metalation can proceed already at room temperature or after moderate annealing.[72,73,83] It was studied in detail for 2HTPP with Co,[4,72,76] Fe,[73,83–85] Ni,[56,78] Cu,[35,36,58,79–82] Zn[32,76,77] and Ce[74,75] on Cu(111), Ag(111) and Au(111). The surface-mediated reaction follows the equation:

$$\mathrm{M(ads)} + \mathrm{2HTPP(ads)} \rightarrow \mathrm{MTPP(ads)} + \mathrm{H_2(g)}$$

with M being the corresponding metal. Presently, no theoretical calculations for this surface reaction are available. In gas phase DFT calculations, the reaction comprises the following elementary steps: (a) coordination of the metal atom by the intact free base porphyrin, 2HTPP, (b) successive transfer of the two hydrogen atoms from the respective nitrogen atoms to the metal atom and (c) formation and release of H_2. Therefore, the transfer of the first hydrogen to the metal was identified as the rate limiting step, which determines the activation energy for the metalation.[76,82] On the surface, the situation may be more complex.

A particularly interesting surface-mediated reaction is the so called self-metalation of free base porphyrins, in which the porphyrin is metalated with a substrate atom of a metal.[35,36,58,79–82] As discussed in the last section, the adsorption behaviour of 2HTPP and metalloporphyrins (*e.g.*, CoTPP), is very different, see Fig. 2. When studying the self-metalation of 2HTPP on Cu(111), this different behaviour makes it possible to discriminate the

reactant 2HTPP from the reaction product CuTPP. As schematically illustrated in Fig. 5a and b, the reactant 2HTPP is comparably immobile while the product CuTPP diffuses very fast (indicated by the horizontal arrows). As a result, CuTPPs cannot be imaged as isolated molecules using STM at room temperature. For low coverage, they can be regarded as 2D gas, and are therefore imaged only as noisy regions, in contrast to the 2HTPPs, which are imaged as individual molecules. The self-metalation reaction of 2HTPP on Cu(111) does not occur at RT but can be thermally activated at around 400 K. In Fig. 5c, an STM image of a 2HTPP layer with a coverage of ρ_0 = 0.135 molecules per nm^2 is shown after adsorption at RT. Fig. 5d and e show the same layer after annealing to 400 K for 42 and 102 min, respectively, and subsequent cooling to RT. Clearly, a pronounced decrease of the 2HTPP density is observed with increasing annealing time. Obviously, at 400 K, the metalation reaction is slow enough to be followed on the time scale of minutes. From Fig. 5c–e it is also evident that individual 2HTPP molecules are clearly distinguishable, which allows us to determine their molecular density and thus to quantitatively follow the isothermal reaction as a function of time. These data measured at different temperatures then provide access to the kinetics of the reaction. The decrease of the 2HTPP density is directly related to the consumption of the reactant in the metalation reaction. In Fig. 6a, the normalized 2HTPP density, ρ_t/ρ_0, is plotted as a function of time for four different temperatures, 390, 395, 400 and 410 K. The data show that, as expected, the density decreases with reaction time at a given temperature, and that the reaction proceeds faster at higher temperatures.

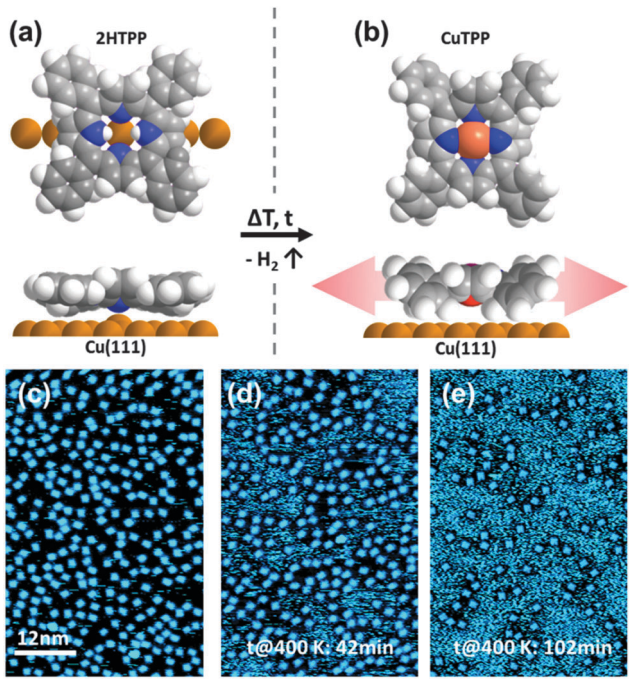

Fig. 5 (a) Due to a strong interaction of the iminic nitrogen atoms of the 2HTPP porphyrin macrocycle with the underlying Cu substrate the molecule is literally pulled towards the surface, thus exhibiting a flat conformation and is rather immobile at RT. (b) For CuTPP all four nitrogen atoms are coordinated equally to the Cu center. As a result, the interaction with the surface is reduced and the molecule is very mobile at RT. (c–e) Constant current room temperature STM images of (c) 2HTPP as prepared on Cu(111) and (d), (e) after annealing to 400 K for the indicated times. The estimated molecular densities of 2HTPP and the corresponding tunnelling parameters are: (c) ρ_0 = 0.135 molecules per nm^2 U = −1.07 V, I = 200 pA; (d) ρ_{42min}@400 K = 0.094 molecules per nm^2, U = −1.20 V, I = 231 pA; (e) ρ_{102min}@400 K = 0.042 molecules per nm^2, U = −1.20 V, I = 230 pA. (Adapted with permission from Ditze *et al.*[35] Copyright 2012 Wiley.)

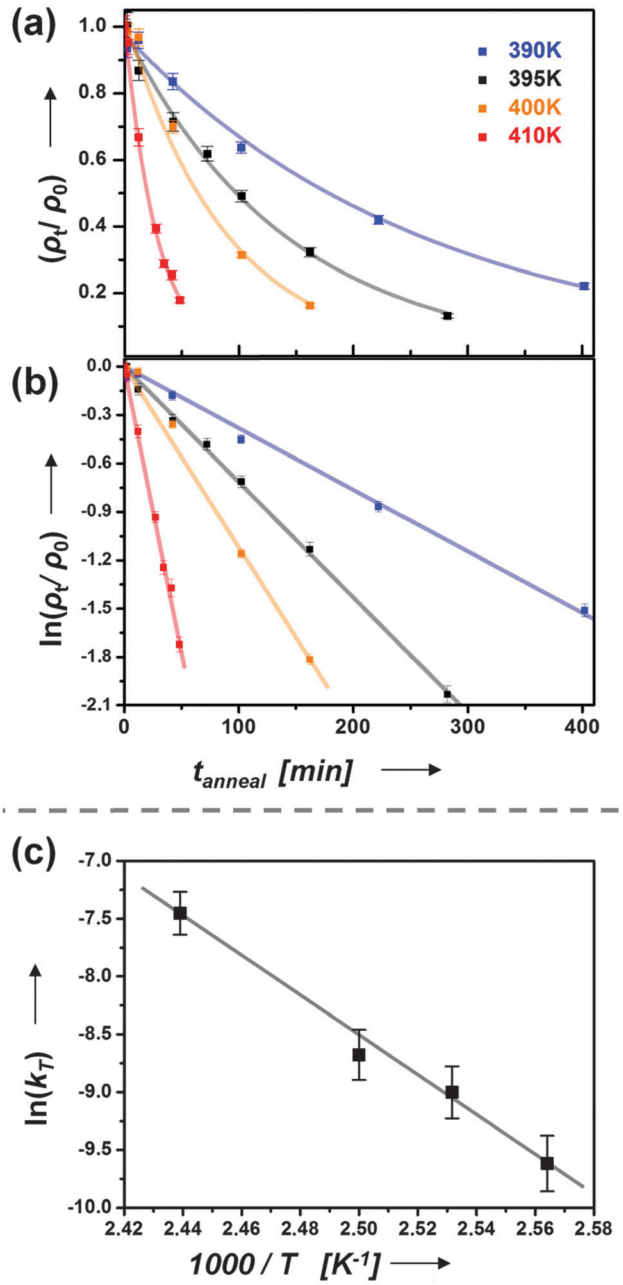

Fig. 6 Graph of normalized molecular density (ρ_t/ρ_0) of 2HTPP on Cu(111) with annealing time at the indicated constant temperatures. (b) Logarithmic plot of the data in (a). (c) Arrhenius plot of the rate constants, k_T, derived from the corresponding line slopes in (b). (Reprinted with permission from Ditze *et al.*[35] Copyright 2012 Wiley.)

The decrease follows an exponential behaviour for all temperatures, which is even more evident from the logarithmic plot in Fig. 6b. This is in perfect agreement with a pseudo first order reaction, according to $\rho_t/\rho_0 = \exp(-k_T \cdot t)$. Such a behaviour is expected, since the Cu(111) crystal represents an infinite reservoir for Cu atoms, *i.e.*, the concentration of available Cu atoms does not change, and consequently the reaction rate is proportional to the concentration of 2HTPP only. The corresponding rate constants, k_T, can be directly determined as the slopes of the fitted lines in Fig. 6b. Using the Arrhenius equation, $k_T = A \cdot \exp(-E_a/k_B T)$, one then obtains the activation energy, E_a, and the preexponential factor, A, by plotting $\ln(k_T)$ *vs.* $1/T$ (Fig. 6c). Linear regression yields $E_a = 1.48 \pm 0.12$ eV and $A = 10^{15\pm1.6}$ s^{-1}.

The presented analysis, which is based on the isothermal "molecule counting" in STM images obtained at different temperatures, is a unique example of the experimental determination of the reaction kinetics and the activation barrier for a surface reaction of larger organic molecules. The estimated activation energy value of $E_a = 1.48 \pm 0.12$ eV is in good agreement with previous DFT calculations of the metalation reaction of the bare free base porphyrin macrocycle with Cu in the gas phase which yielded values ranging from 1.03 to 1.60 eV, depending on the level of theory and applied basis sets.[32,76] The only value of the activation energy of a metalation reaction reported before the work of Ditze *et al.*[35] was derived not from isothermal data, but from a temperature-programmed desorption (TPD) measurement of deuterium during the metalation of 2DTPP (deuterated analogue to 2HTPP) with Zn on Ag(111).[76] Using Redhead's equation,[86] the activation energy was deduced. The major weakness of the Redhead approximation is the fact that the preexponential factor k_0 cannot be determined, but has to be assumed; a value of 10^{13} s^{-1} was used in the corresponding analysis.

It should be noted that for the described temperature-dependent measurements it was crucial that comparable initial coverages were used: in Fig. 6, the 2HTPP starting density, ρ_0, varied between 0.135 and 0.174 molecules per nm^2 (this roughly corresponds to ~23–30% of a saturated monolayer of CuTPP on Cu(111) in a well-ordered quadratic adsorbate lattice). Indeed, it was later shown that while the metalation rate is independent of coverage up to ~0.36 molecules per nm^2, it exhibits an abrupt boost by a factor of 20 above this value,[36] where the transition regime to the formation of a peculiar checkerboard 2HTPP phase occurs.[57]

Possible extensions for future studies of the kinetics of metalation reactions are to investigate the role of the crystallographic orientation of the surface or the study of stepped surfaces, in order to obtain more information on the rate-limiting step. Also, calculations including the Cu surface are highly desired. Furthermore, automated image processing routines are currently developed (see Section 4), which will speed up the analysis significantly (note that for the data plotted in Fig. 6 more than 250 000 2HTPPs were counted by hand). In perspective, the kinetic analysis of isothermal STM experiments might play an important role in gaining a detailed quantitative insight into complex surface reactions in the future.

4 Conformational switching of porphyrin molecules

Last but not least, the thermally and tip induced conformational switching of 2*H*-5,10,15,20-tetrakis-(3,5-di-*tert*-butyl)-phenylporphyrin (2HTTBPP) adsorbed on Cu(111) will be reviewed.[37] Using individual molecules or atoms as functional entities[2,87] is certainly one of the main goals of nanotechnology with the vista to engineer functional devices. One particularly fascinating area is the application of switchable molecular building blocks in information storage.[88,89] In order to achieve this goal, however, a detailed understanding of the adsorption behaviour of large organic molecules on well-defined surfaces is essential, which has stimulated model investigations in an ultra-high vacuum. A large number of studies have been performed using LT STM; this method not only allows for direct imaging of the adsorbed species in real space, but also opens up the possibility to manipulate the molecular objects.[20,27,90–95] A variety of different switching mechanisms has been investigated. These include tautomerization of naphthalocyanine or 2*H*-porphyrin,[19,96] molecular cascades of CO molecules on Cu(111),[97] bond formation or cleavage in adsorbed molecules,[98–100] conformational modifications in general,[62,101,102] and specifically the *trans–cis* conformational changes in azobenzene.[103–105]

Since the activation energies in the mentioned examples are in most of the cases rather small, the corresponding experiments are typically performed at temperatures well below 80 K, in order to prevent unwanted thermally induced activation, and also surface diffusion. The applied low temperatures are certainly not compatible with "real world" applications. To engineer devices suitable for higher temperatures, new molecular building blocks have to be designed and evaluated, and a fundamental understanding of the involved mechanisms is necessary. One promising approach in this context is addressing individual molecules within a self-assembled supramolecular array with a high degree of long range order. In such an arrangement, diffusion can be effectively prevented, and one could envisage tailoring the stability of a certain molecular conformation by the interplay between adsorbate–substrate and adsorbate–adsorbate interactions. Very recently, Ditze *et al.* discovered that 2HTTBPP on Cu(111) is a system which fulfils these criteria.[37] 2HTTBPP is a porphyrin very similar to 2HTPP; it is significantly larger due to the attachment of two *tert*-butyl groups at the 3 and 5 positions of each phenyl substituent, *i.e.*, of altogether eight *tert*-butyl groups. Previous studies on corresponding metallo-TTBPPs reported high conformational flexibility and thus switching capabilities on different substrates.[21,101,102,106,107] On the other hand, the uncoordinated iminic nitrogen atoms of free base porphyrins like 2HTTBPP are expected to form a strong attractive interaction with the Cu substrate;[33,80,81] this type of interaction was already discussed in the previous sections for the smaller 2HTPP.[34–36,58,79,108]

The investigation by Ditze *et al.* indeed reveals that 2HTTBPP exhibits a very unusual and interesting adsorption behaviour. Fig. 7a shows an overview STM image of a sub-monolayer of 2HTTBPP on Cu(111). The molecules are arranged

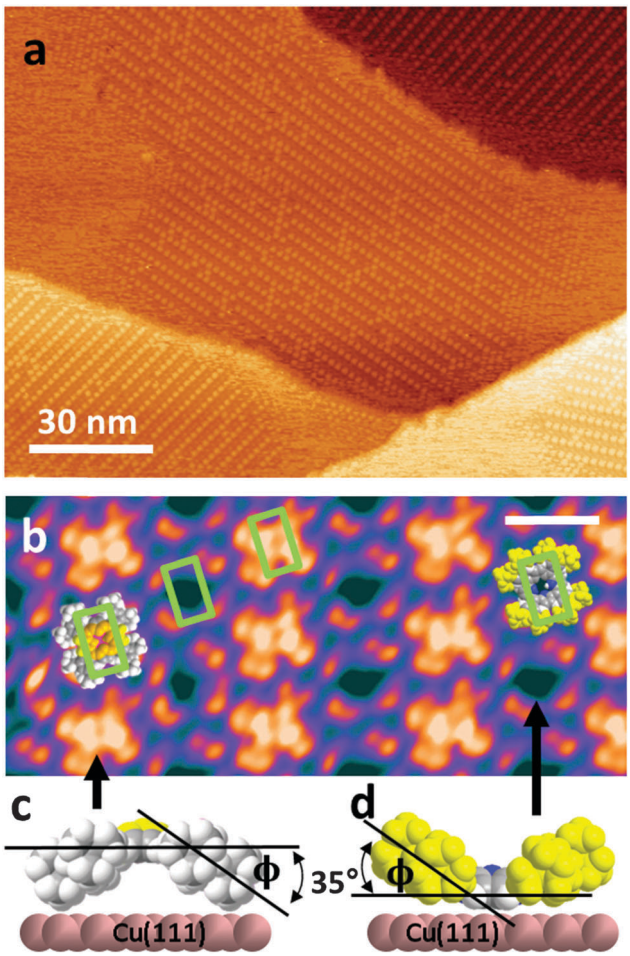

Fig. 7 (a) STM image of ordered domains of 2HTTBPP on Cu(111) acquired at room temperature (U = +1.31 V, I = 30 pA). The molecules exhibit a bimodal appearance, *i.e.*, alternating bright and dark lines/rows are visible in STM. (b) High resolution RT STM image (U = +1.30 V, I = 30 pA) of the supramolecular order shown in a. The bright and dark rows in (a) consist of molecules with different intramolecular conformations, as indicated by the overlaid scaled models (top view). The scale bar represents 2 nm. (c, d) Space filling models of the convex (c) and concave (d) conformations of 2HTTBPP. The determination of the intramolecular conformation is based on the appearance in STM, in particular on the green rectangle formed by the peripheral substituents as indicated in the high resolution ST micrographs. (Adapted with permission from Ditze *et al.*[37] Copyright 2014 American Chemical Society.)

in domains of alternating bright and dark rows. In the high resolution STM image in Fig. 7b one can distinguish two types of appearances of 2HTTBPP: the bright rows consist of molecules with a central protrusion and the dark rows of molecules with a central depression. For both types, the periphery of the molecules appears as eight bright spots, which can be assigned to the eight *tert*-butyl substituents arranged in four groups around the molecular centre corresponding to the four phenyl groups.[21,102,106]

The four peripheral groups form a rectangle (indicated in green), which is identical for the two different molecular appearances. In an earlier study on TTBPPs it was shown that the intramolecular conformation of the molecules can be deduced from the geometry of the rectangle, that is, from the aspect ratio of the short and long sides, and the perimeter.[106] The resulting conformation is described by twisting (by a twist angle θ) and/or tilting of the phenyl rings (by a tilt angle ϕ) with respect to the porphyrin plane; see ref. 37 and 106 for details.

From the image in Fig. 7b, the two angles are estimated to be $\theta = 5 \pm 5^\circ$ and $\phi = 35 \pm 5^\circ$ for both conformations. The value of θ being close to zero is confirmed by the fact that all eight *tert*-butyl substituents appear with a similar apparent height. In a recent gas phase DFT study of the energy surface of the very similar porphyrin CoTTBPP, a local minimum was found at very similar twist and tilt angles ($\theta = 10^\circ$ and $\phi = 30^\circ$), albeit at a relatively high energy.[107] In this conformation the molecule adopts a concave, bowl-like shape. Such conformations, which are rather exotic and energetically unfavourable in the gas-phase, might be stabilized on a surface by molecule–substrate, but also by lateral molecule–molecule interactions. Based on these considerations, the two different appearances of 2HTTBPP on Cu(111) can be understood: the dark molecules are in a concave conformation, *i.e.*, with the bottom of the "bowl" on the surface (Fig. 7d), while the bright molecules are in a convex conformation, *i.e.*, the bowl is upside down (Fig. 7c). This interpretation was fully confirmed by DFT level-simulated STM images of the molecules on a three layer Cu slab.[37]

It is interesting to compare this pronounced bimodal appearance with the behaviour of two closely related systems, namely 2HTTBPP on Ag(111)[109] and CuTTBPP on Cu(111); for the latter a very different geometry ($\theta = 75 \pm 5^\circ$ and $\phi = 0 \pm 5^\circ$) is found, which is very similar to the overall minimum reported for CoTTBPP in the gas phase calculations.[107] The very different behaviour found here for 2HTTBPP on Cu(111) ($\theta = 5 \pm 5^\circ$ and $\phi = 35 \pm 5^\circ$) is a strong indication of considerable stabilizing interactions. For the concave conformation, this interpretation is in line with a strong attractive interaction between the iminic nitrogen atoms and the Cu substrate, by which the porphyrin macrocycle is literally "pulled" towards the surface;[34,35,53,55,79] the reason for the convex conformation, however, is not readily accessible. Here lateral interactions also must play a role and it will be later discussed that this conformation is entropically stabilized.

While the static situation is already peculiar, the dynamic behaviour is even more interesting. From Fig. 7a, it is evident that the order in the dark and bright rows is not perfect. Indeed, inspection of successive STM images of the same surface region at RT shows that individual molecules in both rows occasionally change their appearance from dark to bright and *vice versa*; for better illustration, in Fig. 8 a corresponding image series is shown that was extracted from a high resolution RT STM movie; switching molecules are indicated by the white arrows (see ESI Movie M1 from ref. 37). The observed behaviour demonstrates a spontaneous reversible conformational switching of individual 2HTTBPPs, indicating the metastable nature of the intramolecular conformation at room temperature.

The switching of the molecules between the two conformations in the two rows is attributed to a thermally induced process. By performing measurements at different temperatures, one can then gain access to the corresponding temperature-dependent dynamics

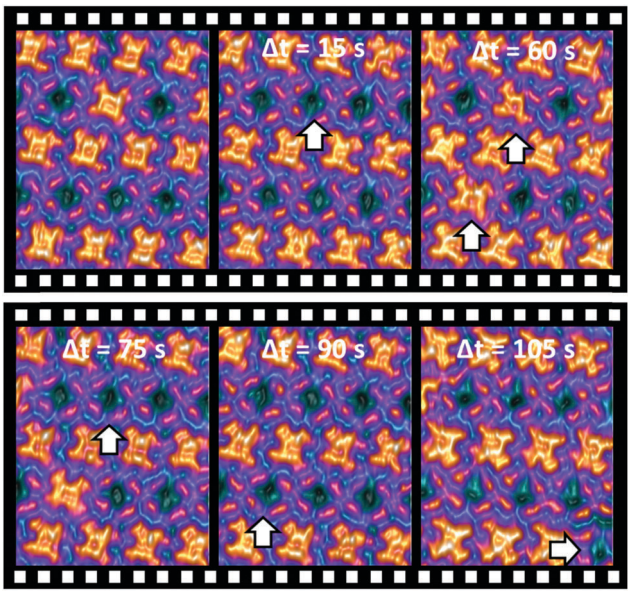

Fig. 8 Selected images from a high resolution STM movie of a 2HTTBPP domain on Cu(111) acquired at RT (image to image acquisition time 15 s; U = +1.76 V, I = 24 pA). The arrows indicate individual molecules which exhibit a spontaneous conformational switching from concave to convex or *vice versa*. The times after acquisition of the first micrograph (left) are indicated by the t values. (Adapted with permission from Ditze *et al.*[37] Copyright 2014 American Chemical Society.)

close to RT, and thereby obtain an understanding of the energetics of the switching. To cover a sufficient temperature range, the measurement time per image has to be comparably short. For the ST micrographs in Fig. 8, the acquisition speed (15 seconds for 12 nm^2 acquired with 512^2 pixels) was not sufficient to track all switching events at RT.

In order to significantly improve the time resolution, the acquisition time for a 12 nm^2 image was reduced from 15 to 1.8 seconds, by reducing the resolution from 512^2 to 128^2 and increasing the scan speed. Even though the spatial resolution of these images is significantly lower, the contrast between concave and convex molecules is still very good.[37]

Using this accelerated data acquisition, time lapse movies were measured between 270 and 320 K, and a specific visualization technique to analyse the time evolution of height profiles was applied.[36] The data show an increase of the switching rate with increasing temperature for both rows, indicative of activated processes. However, when comparing the behaviour in the two rows, it was found that molecules in the concave rows switch much more frequently than those in the convex rows.[37] This is unexpected, since the strong attractive interaction of the iminic nitrogen of the 2HTTBPP with the substrate and significant van der Waals forces[37] suggests a stronger bond and thus a higher energy barrier for switching molecules in the concave row than in the convex row.

Further insight into these thermally driven switching processes is achieved from a quantitative analysis of isothermal time lapse movies, which were acquired at five temperatures between 280 and 300 K. The criterion for the upper limit of 300 K was that the observed switching processes are still slower than the time resolution of ~1.8 s of STM for one frame to ensure that no switching events are missed. The criterion for the lower limit of 280 K was that at lower temperatures the number of switching events was not sufficient for a conclusive analysis. In recorded STM images, switching events from the "native" state to the "deviant" state and back, in both the concave and the convex rows, could be identified. In other words, four different switching events were separately analysed, namely from convex (native state) to concave and back in the bright row, and from concave (native state) to convex and back in the bright row. For this analysis, a semi-automatic image processing tool for STM movies was developed and applied. With this tool more than 1.5 million molecular conformations, from more than 70 000 STM images, were extracted from the movies at different temperatures, yielding more than 10 000 switching events. The switching rates, r, for the four states were determined as the number of switching events for a particular state divided by the lifetime of this state (see ESI of ref. 37 for details). The increase of the switching rates for all four switching events with temperature indicates that the intramolecular conformation changes are activated processes. As discussed in Sections 2 and 3, such activated processes are typically evaluated using an Arrhenius analysis, which yields the activation energy E and the corresponding preexponential factor A. As already discussed in Sections 1 and 2, the drawback of this analysis is that it does not provide direct physical insight into the nature of the preexponential factor. This insight is, however, of particular interest and relevance when major changes in the entropy of the different states occur, as is the case for the system studied here. As already outlined in Section 1, the alternative approach is based on the transition state theory (TST), where the Gibbs energy defines the activation barrier to be overcome.[39] Following a method described in detail by Winzor *et al.*,[110] one uses the logarithmic form of the Eyring equation (see Section 1) divided by T:

$$\ln\left(\frac{r}{T}\right) = \ln\left(\frac{k_B}{h}\right) + \frac{\Delta S^{\#}}{k_B} - \frac{\Delta H^{\#}}{k_B T}.$$

By plotting $\ln(r/T)$ as a function of $1/T$, one can then extract the slope

$$m = -\frac{\Delta H^{\#}}{k_B}$$

and the ordinate intercept

$$y = \ln\left(\frac{k_B}{h}\right) + \frac{\Delta S^{\#}}{k_B}$$

With this analysis, it is possible to directly extract the values of $\Delta H^{\#}$ and $\Delta S^{\#}$. It should be noted that for simplicity the transmission factor κ was not considered here, since it is usually set to $\kappa = 1$ and makes no contribution in the logarithmic form, as $\ln(\kappa) = 0$.[37,110]

In Fig. 9, the corresponding plots are shown for the switching events in the concave rows (left) and the convex rows (right),

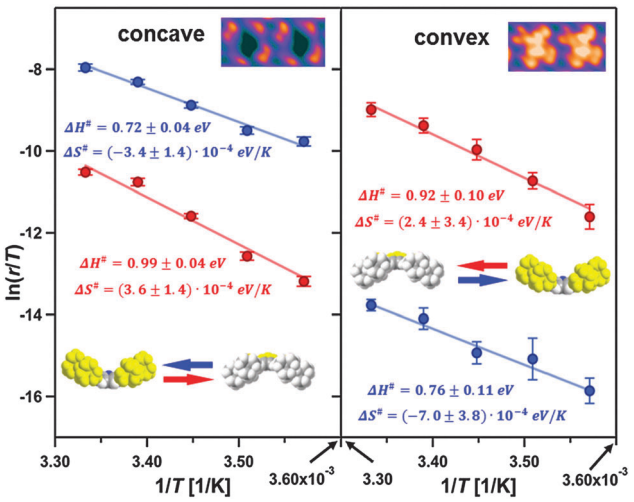

Fig. 9 Plots of ln(*r*/*T*) *vs.* 1/*T* for the two switching events (concave to convex in red, and convex to concave in blue) in the concave row (left-hand side) and in the convex row (right-hand side). The corresponding $\Delta H^{\#}$ and $\Delta S^{\#}$ values determined from linear regressions are given in the same color code. The error bars represent the standard error. (Adapted with permission from Ditze *et al.*[37] Copyright 2014 American Chemical Society.)

as derived from the isothermal STM measurements. For both rows, the data for switching from the concave to the convex conformation and *vice versa* are shown. The lines represent the least square fits; furthermore, the resulting values of $\Delta H^{\#}$ and $\Delta S^{\#}$ are given.

The comparison of the behaviour for the two rows in Fig. 9 shows that the enthalpic barriers for the transition from concave to convex (in red) are the same within the margin of errors ($\Delta H^{\#}$ = 0.92 ± 0.10 for the convex row *vs.* 0.99 ± 0.04 eV for the concave row). The same holds for the reverse switching direction, *i.e.*, from convex to concave (0.76 ± 0.11 *vs.* 0.72 ± 0.04 eV; in blue). In other words, the enthalpic barrier, $\Delta H^{\#}$, is the same for the same transition in the two different rows. The observation that the enthalpic barrier for switching from concave to convex (red) is ~30% higher than for the opposite direction (blue) can be understood, considering the strong attractive interaction of the concave molecule with the substrate. Interestingly and at first sight unexpectedly, despite this stronger interaction, the switching frequency in the concave row is larger than in the convex row; this effect is assigned to entropic contributions.

In Fig. 10, the Gibbs energy scheme, with the derived thermodynamic potentials, $\Delta H^{\#}$ (green), $T\Delta S^{\#}$ (purple) and the resulting barrier $\Delta G^{\#}$ (black), is sketched for 300 K. According to the Gibbs–Helmholtz equation, $\Delta S^{\#}$ contributes to $\Delta G^{\#}$ as $-T\Delta S^{\#}$; thus positive entropy differences lead to a lower Gibbs energy barrier in Fig. 10. We first analyse the behaviour for the convex row (Fig. 10, right). If one only considers $\Delta H^{\#}$ (green), the concave conformation (yellow) would be clearly favoured, which

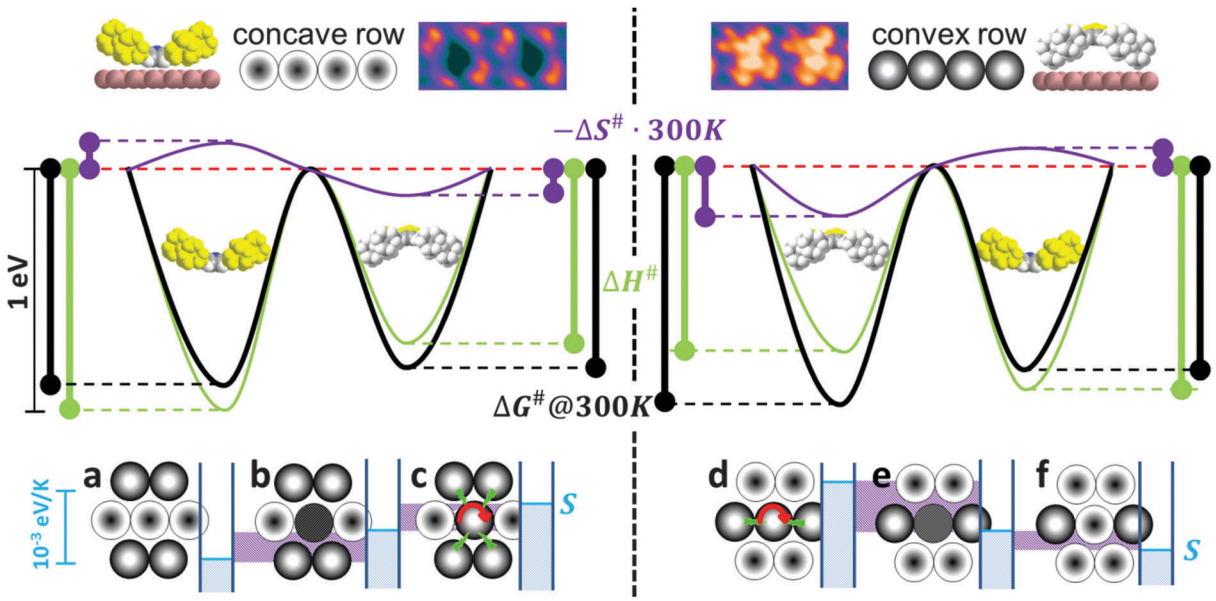

Fig. 10 Sketch of the thermodynamic potential differences at 300 K (vertical bars) and the resulting energy landscape for conformational switching of 2HTTBPP on Cu(111) in the concave (left side) and the convex row (right side). The curve, which determines the switching behaviour, is the one for $\Delta G^{\#}$ drawn in black. The free energy difference is composed of contributions from $\Delta H^{\#}$ and $-\Delta S^{\#}\cdot 300$ K, displayed in green and purple, respectively. Please note that by reducing the temperature the free energy value will shift towards the enthalpy value, *i.e.*, at 0 K the black curve coincides with the green one. In the bottom row, schematic of the central molecule in the convex (c, d: central bright spot), the transition state (b, e: black) and the concave conformation (a, f: central dark spot), along with their next neighbours, is depicted. The height of the blue bar indicates the entropy values *S*, and the purple bars mark the corresponding entropy differences $\Delta S^{\#}$ as extracted from the data depicted in Fig. 9 and directly related to the $-\Delta S^{\#}\cdot 300$ K values above (also printed in purple). The observed entropy increase from concave over the transition state to convex can be explained by the strong molecule–substrate interaction in the concave conformation going along with reduced degrees of freedom. Exemplarily, the rotation of convex molecules is indicated by the red arrows in the scheme (c, d); the green flashes (c, d) indicate steric hindrance by next neighbour molecules with the same convex conformation and thus reduced rotation, *i.e.* smaller entropy. (Reprinted with permission from Ditze *et al.*[37] Copyright 2014 American Chemical Society.)

is expected from the stronger binding to the surface. However, when including the entropic contribution $-T\Delta S^{\#}$ (violet) to the Gibbs energy the convex state becomes favourable (black). This analysis demonstrates that at 300 K convex molecules in the convex rows and thus the whole supramolecular arrangement are entropically stabilized. When analysing the behaviour in the concave row (Fig. 10, left), the entropic contributions also lead to some destabilization of the enthalpically favoured concave conformation (green), but do not reverse the stability in terms of the Gibbs energy (black).

As the next step, we discuss STM results acquired at 200 K. At this temperature, no thermally induced switching between the concave and convex conformations is observed. Nevertheless, the situation is not static: STM movies measured at 200 K reveal that, irrespective of their molecular neighbourhood, convex 2HTTBPP molecules frequently change their appearance and azimuthal orientation. These observations indicate that the molecules can rotate around the surface normal already at 200 K, and that vibrational degrees of freedom and also frustrated translations are excited. In contrast, concave molecules do not change their appearance, which is attributed to the stronger molecule–substrate interaction *via* the iminic nitrogen atoms. This strong interaction not only suppresses rotational motion, but may also result in an enhanced lateral confinement, and possibly also in energetically less accessible vibrational motions due to a stiffening of the whole molecule. Thus, for the convex molecules the entropic contributions of rotational, vibrational, and frustrated translational motions are larger than those for their concave counterparts.

The influence of rotational entropy on the behaviour of larger organic molecules was recently studied by temperature programmed desorption experiments, partially combined with STM.[68,111–113] Waldmann *et al.* observed large differences in the preexponential factor for desorption, depending on the rotational state before desorption:[113] the entropy difference between adsorbed molecules and desorbed molecules in the gas phase was found to be smaller for molecules, which rotate in the adsorbed state, as compared to non-rotating ones. To obtain an estimate for the here studied systems, we follow the route described by Waldmann *et al.*;[113] for the rotational entropy of a 2HTTBPP molecule freely rotating around an axis perpendicular to the surface plane this yields a value of 5.1×10^{-4} eV K^{-1}. This corresponds to a $T\Delta S^{\#}$ value of 0.15 eV at 300 K, and represents the difference between a freely rotating and a non-rotating 2HTTBPP. This certainly has to be considered only as an upper estimate of the actual value, since in the supramolecular structure the convex molecule is not expected to rotate freely. This value is to be compared with the $T\Delta S^{\#}$ difference of 0.28 eV at 300 K, deduced from the entropy difference of the two conformations for the convex row in Fig. 9 (right). The rotational entropy value of 0.15 eV is only $\sim$55% of the measured value. We attribute this difference to the fact that other degrees of freedom, that is, vibrations and frustrated translations, will also contribute to the entropy difference between the two conformations.

In the following analysis, we exemplarily focus on the rotation to obtain a qualitative picture of the entropy differences. The bottom part of Fig. 10 schematically illustrates the explanation for the entropy differences by considering one specific molecule (in the center) with its six next neighbours. Our conjecture is that the more strongly bound concave molecules (a, f) generally have much smaller entropy than the convex ones (c, d), which are able to rotate in the supramolecular structure (indicated by red arrows). Therefore neighbouring molecules can be considered as ''bearing'' for the rotational motion.[114] From our data and simple steric considerations we propose that neighbours with the same conformation hinder rotation, and also other motions, due to steric repulsions. Hence, for a convex molecule, with an increasing number of convex next neighbours (indicated with green flashes in c, d) the degree of freedom of rotational motion will be increasingly frustrated and thus the entropy will decrease. In other words, the rotational entropy of a convex molecule with convex neighbours in the neighbouring rows (c) is lower than that of a convex molecule which has only two convex neighbours (d). Based on these considerations, *i.e.*, by accounting for the conformation of the central molecules and their neighbours, the relative magnitude of the entropies from Fig. 9 (indicated by the blue horizontal bars at the right side of the structures) can be understood (a)–(f).

In addition to the detailed analysis of thermally induced switching close to RT, Ditze *et al.* also demonstrated the intentional switching of selected individual porphyrin molecules with the STM tip at 200 K; at this temperature, thermally induced switching is completely suppressed.[37] Interestingly, only convex molecules could be switched to the concave conformation, by applying bias pulses (*e.g.*, +1.75 V for 5 seconds with closed feedback loop maintaining I = 30 pA) while the reverse process was not possible. This behaviour can partly be understood considering that the entropic contributions to the activation barrier decrease with temperature, and thus the energy landscape of the free energy (black in Fig. 10) will shift towards the enthalpy contribution (green in Fig. 10) until both curves merge at 0 K. In other words, both the entropic stabilization of the convex conformation and the entropic destabilization of the concave conformation decrease with decreasing temperature. Thus, at lower temperatures, the concave conformation becomes increasingly favourable also in the convex row. As a consequence, the free energy barrier for switching from convex to concave is reduced and thus the corresponding tip-induced switching is facilitated. Apart from this thermodynamic argument, one also has to consider the tip-induced switching results from the impact of the tunnelling electron. Therefore, the cross sections for inelastic electron excitations or relaxation channels for excited states in the molecule will play an important role. With respect to the latter, the strong coupling of the concave molecules to the substrate could provide an effective decay channel for tip-induced excitations, which leads to a quenching of the switching from concave to the convex conformation.

Finally, it is interesting to note that consecutive switching of directly neighbouring molecules in a convex row leads to the destruction of the local supramolecular order. However, switching every second molecule in the convex row leaves the supramolecular arrangement intact. Thus, a maximum

information storage density of 4.9×10^{13} bit per inch^2 can be achieved with 2HTTBPP on Cu(111).

To conclude this section, the presented example not only provides detailed insights into thermally induced switching and the role of entropic effects, but also underlines the potential and importance of corresponding RT measurements, in particular for systems with energetic landscapes that have the potential for room temperature applications. Furthermore, the results also considerably expand the field of STM tip-induced molecular switching to higher temperatures, which is a crucial and important step towards devices for room temperature applications.

5 Conclusions and outlook

In this feature, three different case studies were reviewed which, based on isothermal STM measurements in UHV, provide insight into the dynamics of diffusion, reactions and molecular switching at surfaces. The reviewed examples demonstrate that variable temperature STM can be a suitable tool to directly monitor the dynamic behaviour of individual adsorbed molecules, at and close to room temperature. In all cases, the behaviour of the free base porphyrins 2HTPP and 2HTTBPP on Cu(111) was investigated. These systems proved to be particularly suitable for such studies, due to the strong bonding interaction of the iminic nitrogen atoms in the porphyrin macrocycle with the Cu substrate atoms. As a consequence, the corresponding activation energies for diffusion, reaction and switching are of a magnitude that allows following the processes at around room temperature, in contrast to most previous studies, which were performed at cryogenic temperatures.

The first example addressed the surface diffusion of 2HTPP on Cu(111). For this system, individual isolated 2HTPP molecules can be observed by standard STM at RT and their migration on the surface can be traced accurately. This gives access to temperature-dependent measurements of the dynamic behaviour at and close to RT, namely diffusion and rotation. Using an Arrhenius analysis, the activation barrier for migration was determined to be $E_m = 0.71 \pm 0.08$ eV, with a preexponential factor $A_m = 10^{10.9\pm1.4}$ s^{-1}. In an analogous way the activation barrier for the rotation of the migration direction by $\pm 120^\circ$ was determined to be $E_r = 1.28 \pm 0.12$ eV, with a preexponential factor of $A_r = 10^{17.0\pm1.8}$ s^{-1}. The adsorption behaviour is strongly modified if a metal center is complexed in the porphyrin macrocycle, coordinated to all four nitrogen, which considerably weakens the molecule–substrate interaction as compared to 2HTPP. Consequently, metalloporphyrins such as CuTPP or CoTPP diffuse much faster at RT such that they cannot be imaged as an isolated species anymore.

The second example dealt with the self-metalation of 2HTPP on Cu(111). By heating the sample to temperatures at around 400 K, the insertion of a Cu atom into the porphyrin macrocycle, that is, the formation of CuTPP, is thermally induced. The progress of the reaction was followed by subsequent imaging the surface, and counting the remaining 2HTPPs, as a function of annealing time at the elevated temperature. By performing such measurements for different annealing temperatures between 390 and 410 K, the kinetics of the self-metalation reaction was studied. From an Arrhenius analysis, the activation energy and the preexponential factor were determined to be $E_a = 1.48 \pm 0.12$ eV and $A = 10^{15\pm1.6}$ s^{-1}, respectively.

In the third example, we reviewed the thermally induced conformational switching of 2HTTBPP on Cu(111). Upon adsorption at room temperature, 2HTTBPPs self-assemble into a long-range ordered structure, with a bimodal appearance in STM. This specific structure is attributed to alternating rows of molecules with concave and convex intramolecular conformation. For both rows, switching between the concave and convex conformation is observed at around room temperature. In order to study the energetics of this thermally induced switching process, temperature-dependent measurements were performed between 280 and 300 K. The analysis of the corresponding kinetic data for this example was not performed using an Arrhenius analysis, but in the framework of transition state theory, based on the Eyring equation. From this analysis of the free energy landscape, a more detailed insight into interpretable thermodynamic potentials can be obtained. In particular, the entropy gain and the enthalpic barrier for the different switching processes were determined. The extracted values evidence a dominating role of entropic effects in the system at room temperature. In the alternative Arrhenius analysis such entropic effects find their analogue in differences in the preexponential factors. These can also be transformed into the corresponding entropy values, as shown by Eichberger *et al.*, when investigating an unexpectedly fast surface diffusion of 2HTPyP dimers on Cu(111).[33]

As an outlook, we want to stress the importance of the results by Buchner *et al.*,[34] Eichberger *et al.*[33] and Ditze *et al.*[37] achieved by UHV STM, which demonstrate that entropic effects have to be generally considered for large organic molecules on surfaces at and close to RT. The general character of these investigations is underlined by recent STM experiments at the liquid/solid interface. Friesen *et al.* investigated the dynamics of reversible binding of O_2 at the metal centre of cobaltoctaethylporphyrin,[115] and Blunt *et al.* studied the dynamics of reversible transformation of two supramolecular phases of an alkylated dehydrobenzo[12]annulene derivative[116] in solution on an HOPG surface. In temperature- and concentration-dependent STM studies, the entropic and enthalpic contributions were estimated and the authors also report significant contributions from entropy close to RT.[115,116] Overall, the discussed examples clearly indicate the necessity to further investigate fundamental questions concerning the role of the thermodynamic potentials, in particular of entropic effects, in such processes. From an application point of view, there is an urgent need to further explore supramolecular systems with specifically tailored organic molecules at RT, in order to evaluate their potential as functional building blocks in room temperature applications. Here, strong collaborations with synthetic chemistry and theory are required, in order to tailor molecules that are suitable, *e.g.*, for switching at and preferably even above room temperature.

Acknowledgements

The authors gratefully acknowledge the funding of the German Research Council (DFG) by the Collaborative Research Center 583 and by the Cluster of Excellence 'Engineering of Advanced Materials' (http://www.eam.uni-erlangen.de) at the Friedrich-Alexander-Universität Erlangen-Nürnberg. They are also very grateful to their former and present coworkers and students, Dr F. Buchner, Dr S. Ditze, M. Stark, Dr K. Comanici, Dr E. Zillner, M. Drost, M. Röckert, Dr J. Xiao, M. Chen, Dr O. Lytken, Prof. J. M. Gottfried, N. Luckas, Dr W. Hieringer, Prof. A. Görling, Prof. N. Jux, A. Aichert and Prof. J. Hornegger, for their excellent work and the fruitful collaboration.

Notes and references

1 G. Binnig, H. Rohrer, C. Gerber and E. Weibel, *Phys. Rev. Lett.*, 1982, **49**, 57–61.
2 J. V. Barth, G. Costantini and K. Kern, *Nature*, 2005, **437**, 671–679.
3 J. V. Barth, J. Weckesser, N. Lin, A. Dmitriev and K. Kern, *Appl. Phys. A: Mater. Sci. Process.*, 2003, **76**, 645–652.
4 J. M. Gottfried and H. Marbach, *Z. Phys. Chem.*, 2009, **223**, 53–74.
5 L. R. Milgrom, *The Colours of Life*, Oxford University Press, 1997.
6 *The Porphyrin Handbook Vol. 4: Biochemistry and Binding: Activation of Small Molecules*, ed. K. M. Kadish, K. M. Smith and R. Guilard, Academic Press, San Diego, 2000.
7 *The Porphyrin Handbook Vol. 13: Chlorophylls and Bilins: Biosynthesis, Synthesis, and Degradation*, ed. K. M. Kadish, K. M. Smith and R. Guilard, Academic Press, San Diego, 2003.
8 N. A. Rakow and K. S. Suslick, *Nature*, 2000, **406**, 710–713.
9 G. Guillaud, J. Simon and J. P. Germain, *Coord. Chem. Rev.*, 1998, **178–180**, 1433–1484.
10 S. Kang, M. Yasuda, H. Miyasaka, H. Hayashi, M. Kawasaki, T. Umeyama, Y. Matano, K. Yoshida, S. Isoda and H. Imahori, *ChemSusChem*, 2008, **1**, 254–261.
11 L. Y. Luo, C. F. Lo, C. Y. Lin, I. J. Chang and E. W. G. Diau, *J. Phys. Chem. B*, 2006, **110**, 410–419.
12 M. Morisaki, K. Enomoto, T. Ito, I. Tabata, K. Hisada and T. Hori, *Sen'i Gakkaishi*, 2007, **63**, 301–306.
13 L. Schmidt-Mende, W. M. Campbell, Q. Wang, K. W. Jolley, D. L. Officer, M. K. Nazeeruddin and M. Grätzel, *ChemPhysChem*, 2005, **6**, 1253–1258.
14 Q. Wang, W. M. Campbell, E. E. Bonfantani, K. W. Jolley, D. L. Officer, P. J. Walsh, K. Gordon, R. Humphry-Baker, M. K. Nazeeruddin and M. Grätzel, *J. Phys. Chem. B*, 2005, **109**, 15397–15409.
15 J. H. Yum, S. R. Jang, R. Humphry-Baker, M. Grätzel, J. J. Cid, T. Torres and M. K. Nazeeruddin, *Langmuir*, 2008, **24**, 5636–5640.
16 J. V. Barth, *Annu. Rev. Phys. Chem.*, 2007, **58**, 375–407.
17 J. Otsuki, *Coord. Chem. Rev.*, 2010, **254**, 2311–2341.
18 W. Auwärter, F. Klappenberger, A. Weber-Bargioni, A. Schiffrin, T. Strunskus, C. Wöll, Y. Pennec, A. Riemann and J. V. Barth, *J. Am. Chem. Soc.*, 2007, **129**, 11279–11285.
19 W. Auwärter, K. Seufert, F. Bischoff, D. Écija, S. Vijayaraghavan, S. Joshi, F. Klappenberger, N. Samudrala and J. V. Barth, *Nat. Nanotechnol.*, 2012, **7**, 41–46.
20 X. H. Qiu, G. V. Nazin and W. Ho, *Science*, 2003, **299**, 542–546.
21 T. A. Jung, R. R. Schlittler and J. K. Gimzewski, *Nature*, 1997, **386**, 696–698.
22 H. Spillmann, A. Kiebele, M. Stöhr, T. A. Jung, D. Bonifazi, F. Y. Cheng and F. Diederich, *Adv. Mater.*, 2006, **18**, 275–279.
23 M. Stöhr, M. Wahl, H. Spillmann, L. H. Gade and T. A. Jung, *Small*, 2007, **3**, 1336–1340.
24 N. Wintjes, D. Bonifazi, F. Y. Cheng, A. Kiebele, M. Stöhr, T. Jung, H. Spillmann and F. Diederich, *Angew. Chem., Int. Ed.*, 2007, **46**, 4089–4092.
25 N. Wintjes, J. Hornung, J. Lobo-Checa, T. Voigt, T. Samuely, C. Thilgen, M. Stöhr, F. Diederich and T. A. Jung, *Chem. – Eur. J.*, 2008, **14**, 5794–5802.
26 L. A. Fendt, M. Stöhr, N. Wintjes, M. Enache, T. A. Jung and F. Diederich, *Chem. – Eur. J.*, 2009, **15**, 11139–11150.
27 Y. F. Wang, J. Kröger, R. Berndt and W. A. Hofer, *J. Am. Chem. Soc.*, 2009, **131**, 3639–3643.
28 L. Grill, K. H. Rieder, F. Moresco, G. Rapenne, S. Stojkovic, X. Bouju and C. Joachim, *Nat. Nanotechnol.*, 2007, **2**, 95–98.
29 V. Arima, R. L. R. Blyth, F. Matino, L. Chiodo, T. Della Sala, J. Thompson, T. Regier, R. Del Sole, G. Mele, G. Vasapollo, R. Cingolani and R. Rinaldi, *Small*, 2008, **4**, 497–506.
30 F. Matino, G. Schull, U. Jana, F. Köhler, R. Berndt and R. Herges, *Chem. Commun.*, 2010, **46**, 6780–6782.
31 K. Flechtner, A. Kretschmann, H.-P. Steinrück and J. M. Gottfried, *J. Am. Chem. Soc.*, 2007, **129**, 12110–12111.
32 A. Kretschmann, M.-M. Walz, K. Flechtner, H.-P. Steinrück and J. M. Gottfried, *Chem. Commun.*, 2007, 568–570.
33 M. Eichberger, M. Marschall, J. Reichert, A. Weber-Bargioni, W. Auwärter, R. L. C. Wang, H. J. Kreuzer, Y. Pennec, A. Schiffrin and J. V. Barth, *Nano Lett.*, 2008, **8**, 4608–4613.
34 F. Buchner, J. Xiao, E. Zillner, M. Chen, M. Röckert, S. Ditze, M. Stark, H.-P. Steinrück, J. M. Gottfried and H. Marbach, *J. Phys. Chem. C*, 2011, **115**, 24172–24177.
35 S. Ditze, M. Stark, M. Drost, F. Buchner, H.-P. Steinrück and H. Marbach, *Angew. Chem., Int. Ed.*, 2012, **51**, 10898–10901.
36 M. Röckert, S. Ditze, M. Stark, J. Xiao, H.-P. Steinrück, H. Marbach and O. Lytken, *J. Phys. Chem. C*, 2014, **118**, 1661–1667.
37 S. Ditze, M. Stark, F. Buchner, A. Aichert, N. Jux, N. Luckas, A. Görling, W. Hieringer, J. Hornegger, H.-P. Steinrück and H. Marbach, *J. Am. Chem. Soc.*, 2014, 1609–1616.
38 S. Arrhenius, *Z. Phys. Chem.*, 1889, **4**, 226–248.
39 K. J. Laidler, S. Glasstone and H. Eyring, *J. Chem. Phys.*, 1940, **8**, 659–667.
40 S. de Feyter and F. C. de Schryver, *Chem. Soc. Rev.*, 2003, **32**, 139–150.
41 E. Ganz, S. K. Theiss, I.-S. Hwang and J. Golovchenko, *Phys. Rev. Lett.*, 1992, **68**, 1567–1570.
42 B. S. Swartzentruber, *Phys. Rev. Lett.*, 1996, **76**, 459–462.
43 T. Zambelli, J. Trost, J. Wintterlin and G. Ertl, *Phys. Rev. Lett.*, 1996, **76**, 795–798.
44 T. R. Linderoth, S. Horch, E. Laegsgaard, I. Stensgaard and F. Besenbacher, *Phys. Rev. Lett.*, 1997, **78**, 4978–4981.
45 J. V. Barth, H. Brune, B. Fischer, J. Weckesser and K. Kern, *Phys. Rev. Lett.*, 2000, **84**, 1732–1735.
46 F. Rosei, M. Schunack, Y. Naitoh, P. Jiang, A. Gourdon, E. Laegsgaard, I. Stensgaard, C. Joachim and F. Besenbacher, *Prog. Surf. Sci.*, 2003, **71**, 95–146.
47 M. Schunack, T. R. Linderoth, F. Rosei, E. Laegsgaard, I. Stensgaard and F. Besenbacher, *Phys. Rev. Lett.*, 2002, **88**, 156102–156106.
48 K.-Y. Kwon, K. L. Wong, G. Pawin, L. Bartels, S. Stolbov and T. S. Rahman, *Phys. Rev. Lett.*, 2005, **95**, 166101–166105.
49 J. Weckesser, J. V. Barth and K. Kern, *J. Chem. Phys.*, 1999, **110**, 5351–5354.
50 J. Weckesser, A. De Vita, J. V. Barth, C. Cai and K. Kern, *Phys. Rev. Lett.*, 2001, **87**, 096101.
51 T. Yokoyama, T. Takahashi and K. Shinozaki, *Phys. Rev. B: Condens. Matter Mater. Phys.*, 2010, **82**, 155414.
52 F. Buchner, I. Kellner, W. Hieringer, A. Görling, H.-P. Steinrück and H. Marbach, *Phys. Chem. Chem. Phys.*, 2010, **12**, 13082–13090.
53 G. Rojas, X. Chen, C. Bravo, J.-H. Kim, J.-S. Kim, J. Xiao, P. A. Dowben, Y. Gao, X. C. Zeng, W. Choe and A. Enders, *J. Phys. Chem. C*, 2010, **114**, 9408–9415.
54 G. Rojas, S. Simpson, X. Chen, D. A. Kunkel, J. Nitz, J. Xiao, P. A. Dowben, E. Zurek and A. Enders, *Phys. Chem. Chem. Phys.*, 2012, **14**, 4971–4976.
55 F. Buchner, E. Zillner, M. Röckert, S. Gläßel, H.-P. Steinrück and H. Marbach, *Chem. – Eur. J.*, 2011, **17**, 10226–10229.
56 S. Ditze, M. Röckert, F. Buchner, E. Zillner, M. Stark, H.-P. Steinrück and H. Marbach, *Nanotechnology*, 2013, **24**, 115305–115316.
57 M. Stark, S. Ditze, M. Drost, F. Buchner, H.-P. Steinrück and H. Marbach, *Langmuir*, 2013, **29**, 4104–4110.
58 J. Xiao, S. Ditze, M. Chen, F. Buchner, M. Stark, M. Drost, H.-P. Steinrück, J. M. Gottfried and H. Marbach, *J. Phys. Chem. C*, 2012, **116**, 12275–12282.
59 J. Brede, M. Linares, S. Kuck, J. Schwöbel, A. Scarfato, S. H. Chang, G. Hoffmann, R. Wiesendanger, R. Lensen, P. H. J. Kouwer,

J. Hoogboom, A. E. Rowan, M. Bröring, M. Funk, S. Stafström, F. Zerbetto and R. Lazzaroni, *Nanotechnology*, 2009, **20**, 275602.
60 G. Rojas, X. Chen, C. Bravo, J. H. Kim, J. S. Kim, J. Xiao, P. A. Dowben, Y. Gao, X. C. Zeng, W. Choe and A. Enders, *J. Phys. Chem. C*, 2010, **114**, 9408–9415.
61 F. Buchner, V. Schwald, K. Comanici, H.-P. Steinrück and H. Marbach, *ChemPhysChem*, 2007, **8**, 241–243.
62 H. Yanagi, H. Mukai, K. Ikuta, T. Shibutani, T. Kamikado, S. Yokoyama and S. Mashiko, *Nano Lett.*, 2002, **2**, 601–604.
63 S. Berner, M. Brunner, L. Ramoino, H. Suzuki, H. J. Güntherodt and T. A. Jung, *Chem. Phys. Lett.*, 2001, **348**, 175–181.
64 J. Weckesser, J. V. Barth and K. Kern, *Phys. Rev. B: Condens. Matter Mater. Phys.*, 2001, **64**, 161403.
65 J. V. Barth, *Surf. Sci. Rep.*, 2000, **40**, 75–149.
66 R. Zacharia, H. Ulbricht and T. Hertel, *Phys. Rev. B: Condens. Matter Mater. Phys.*, 2004, **69**, 155406.
67 M. Roos, A. Breitruck, H. E. Hoster and R. J. Behm, *Phys. Chem. Chem. Phys.*, 2010, **12**, 818–822.
68 S. L. Tait, Z. Dohnalek, C. T. Campbell and B. D. Kay, *J. Chem. Phys.*, 2005, **122**, 164708–164713.
69 S. L. Tait, Z. Dohnalek, C. T. Campbell and B. D. Kay, *J. Chem. Phys.*, 2006, **125**, 234308.
70 M. Wahl, M. Stöhr, H. Spillmann, T. A. Jung and L. H. Gade, *Chem. Commun.*, 2007, 1349–1351.
71 B. G. Briner, M. Döring, H.-P. Rust and A. M. Bradshaw, *Science*, 1997, **278**, 257–260.
72 J. M. Gottfried, K. Flechtner, A. Kretschmann, T. Lukasczyk and H.-P. Steinrück, *J. Am. Chem. Soc.*, 2006, **128**, 5644–5645.
73 W. Auwärter, A. Weber-Bargioni, S. Brink, A. Riemann, A. Schiffrin, M. Ruben and J. V. Barth, *ChemPhysChem*, 2007, **8**, 250–254.
74 A. Weber-Bargioni, J. Reichert, A. P. Seitsonen, W. Auwärter, A. Schiffrin and J. V. Barth, *J. Phys. Chem. C*, 2008, **112**, 3453–3455.
75 D. Écija, W. Auwärter, S. Vijayaraghavan, K. Seufert, F. Bischoff, K. Tashiro and J. V. Barth, *Angew. Chem., Int. Ed.*, 2011, **50**, 3872–3877.
76 T. E. Shubina, H. Marbach, K. Flechtner, A. Kretschmann, N. Jux, F. Buchner, H.-P. Steinrück, T. Clark and J. M. Gottfried, *J. Am. Chem. Soc.*, 2007, **129**, 9476–9483.
77 K. Flechtner, A. Kretschmann, L. R. Bradshaw, M. M. Walz, H.-P. Steinrück and J. M. Gottfried, *J. Phys. Chem. C*, 2007, **111**, 5821–5824.
78 M. Chen, X. F. Feng, L. Zhang, H. X. Ju, Q. Xu, J. F. Zhu, J. M. Gottfried, K. Ibrahim, H. J. Qian and J. O. Wang, *J. Phys. Chem. C*, 2010, **114**, 9908–9916.
79 K. Diller, F. Klappenberger, M. Marschall, K. Hermann, A. Nefedov, C. Woll and J. V. Barth, *J. Chem. Phys.*, 2012, **136**, 014705.
80 R. González-Moreno, C. Sánchez-Sánchez, M. Trelka, R. Otero, A. Cossaro, A. Verdini, L. Floreano, M. Ruiz-Bermejo, A. Garcia-Lekue, J. A. Martín-Gago and C. Rogero, *J. Phys. Chem. C*, 2011, **115**, 6849–6854.
81 S. Haq, F. Hanke, M. S. Dyer, M. Persson, P. Iavicoli, D. B. Amabilino and R. Raval, *J. Am. Chem. Soc.*, 2011, **133**, 12031–12039.
82 Y. Li, J. Xiao, T. E. Shubina, M. Chen, Z. L. Shi, M. Schmid, H.-P. Steinrück, J. M. Gottfried and N. Lin, *J. Am. Chem. Soc.*, 2012, **134**, 6401–6408.
83 F. Buchner, V. Schwald, K. Comanici, H.-P. Steinrück and H. Marbach, *ChemPhysChem*, 2007, **8**, 241–243.
84 F. Buchner, I. Kellner, H.-P. Steinrück and H. Marbach, *Z. Phys. Chem.*, 2009, **223**, 131–144.
85 F. Buchner, K. Flechtner, Y. Bai, E. Zillner, I. Kellner, H.-P. Steinrück, H. Marbach and J. M. Gottfried, *J. Phys. Chem. C*, 2008, **112**, 15458–15465.
86 P. A. Redhead, *Vacuum*, 1962, **12**, 203–211.
87 C. Joachim, J. K. Gimzewski and A. Aviram, *Nature*, 2000, **408**, 541–548.
88 R. L. Carroll and C. B. Gorman, *Angew. Chem., Int. Ed.*, 2002, **41**, 4378–4400.
89 J. E. Green, J. Wook Choi, A. Boukai, Y. Bunimovich, E. Johnston-Halperin, E. DeIonno, Y. Luo, B. A. Sheriff, K. Xu, Y. Shik Shin, H.-R. Tseng, J. F. Stoddart and J. R. Heath, *Nature*, 2007, **445**, 414–417.
90 J. S. Foster, J. E. Frommer and P. C. Arnett, *Nature*, 1988, **331**, 324–326.
91 L. Grill, *J. Phys.: Condens. Matter*, 2008, **20**, 053001.
92 W. Ho, *J. Chem. Phys.*, 2002, **117**, 11033–11061.
93 G. V. Nazin, X. H. Qiu and W. Ho, *Science*, 2003, **302**, 77–81.
94 J. Schaffert, M. C. Cottin, A. Sonntag, H. Karacuban, C. A. Bobisch, N. Lorente, J.-P. Gauyacq and R. Möller, *Nat. Mater.*, 2013, **12**, 223–227.
95 K. Morgenstern, *Surf. Interface Anal.*, 2010, **42**, 1634–1636.
96 P. Liljeroth, J. Repp and G. Meyer, *Science*, 2007, **317**, 1203–1206.
97 A. J. Heinrich, C. P. Lutz, J. A. Gupta and D. M. Eigler, *Science*, 2002, **298**, 1381–1387.
98 P. Maksymovych, D. C. Sorescu, K. D. Jordan and J. T. Yates, *Science*, 2008, **322**, 1664–1667.
99 F. Mohn, J. Repp, L. Gross, G. Meyer, M. S. Dyer and M. Persson, *Phys. Rev. Lett.*, 2010, **105**, 266102.
100 M. Piantek, G. Schulze, M. Koch, K. J. Franke, F. Leyssner, A. Krüger, C. Navio, J. Miguel, M. Bernien, M. Wolf, W. Kuch, P. Tegeder and J. I. Pascual, *J. Am. Chem. Soc.*, 2009, **131**, 12729–12735.
101 C. Loppacher, M. Guggisberg, O. Pfeiffer, E. Meyer, M. Bammerlin, R. Luthi, R. Schlittler, J. K. Gimzewski, H. Tang and C. Joachim, *Phys. Rev. Lett.*, 2003, **90**, 066107.
102 F. Moresco, G. Meyer, K. H. Rieder, H. Tang, A. Gourdon and C. Joachim, *Phys. Rev. Lett.*, 2001, **86**, 672–675.
103 M. Alemani, M. V. Peters, S. Hecht, K.-H. Rieder, F. Moresco and L. Grill, *J. Am. Chem. Soc.*, 2006, **128**, 14446–14447.
104 A. Safiei, J. Henzl and K. Morgenstern, *Phys. Rev. Lett.*, 2010, **104**, 216102.
105 M. Wolf and P. Tegeder, *Surf. Sci.*, 2009, **603**, 1506–1517.
106 F. Buchner, K. Comanici, N. Jux, H.-P. Steinrück and H. Marbach, *J. Phys. Chem. C*, 2007, **111**, 13531–13538.
107 T. Wölfle, A. Görling and W. Hieringer, *Phys. Chem. Chem. Phys.*, 2008, **10**, 5739–5742.
108 M. Stark, S. Ditze, M. Drost, F. Buchner, H.-P. Steinrück and H. Marbach, *Langmuir*, 2013, **29**, 4104–4110.
109 F. Buchner, *STM Investigation of Molecular Architectures of Porphyrinoids on a Ag(111) Surface*, Springer, 2010.
110 D. J. Winzor and C. M. Jackson, *J. Mol. Recognit.*, 2006, **19**, 389–407.
111 C. T. Campbell and J. R. V. Sellers, *J. Am. Chem. Soc.*, 2012, **134**, 18109–18115.
112 K. R. Paserba and A. J. Gellman, *Phys. Rev. Lett.*, 2001, **86**, 4338–4341.
113 T. Waldmann, J. Klein, H. E. Hoster and R. J. Behm, *ChemPhysChem*, 2013, **14**, 162–169.
114 J. K. Gimzewski, C. Joachim, R. R. Schlittler, V. Langlais, H. Tang and I. Johannsen, *Science*, 1998, **281**, 531–533.
115 B. A. Friesen, A. Bhattarai, U. Mazur and K. W. Hipps, *J. Am. Chem. Soc.*, 2012, **134**, 14897–14904.
116 M. O. Blunt, J. Adisoejoso, K. Tahara, K. Katayama, M. Van der Auweraer, Y. Tobe and S. De Feyter, *J. Am. Chem. Soc.*, 2013, **135**, 12068–12075.

